International Journal of Bifurcation and Chaos, Vol. 21, No. 12 (2011) 3549–3556

DOI: 10.1142/S0218127411030714

CLIMATE MODE COVARIABILITY AND CLIMATE SHIFTS

ANASTASIOS A. TSONIS* and KYLE L. SWANSON†
Department of Mathematical Sciences,
Atmospheric Sciences Group,
University of Wisconsin-Milwaukee,
Milwaukee, WI 53217, USA
**aatsonis@uwm.edu*
†*kswanson@uwm.edu*

Received September 3, 2010; Revised January 12, 2011

It has previously been shown from the collective behavior of a network of observed climate indices that this network synchronized several times in the period 1900–2000. Further, it has been found that in those cases where the synchronous state was followed by a steady increase in the coupling strength between the indices, the synchronous state was destroyed, after which a new climate state emerged. These shifts are associated with significant changes in global temperature trend and in El Niño/Southern Oscillation variability. Subsequently, the evidence for such type of behavior has been found to occur in three climate simulations using state-of-the-art models as well as in the observed data in the 21st century. This was the first time that this mechanism, which appears consistent with the theory of synchronized chaos, has been discovered in a physical system of the size and complexity of the climate system. Here we extend this approach to consider proxy data for climate modes going back several centuries. While noise in the proxy data in some cases masks the mechanism, we find significant coherence between both synchronization and coupling and global temperature. These results provide further support that the above mechanism for climate shifts is a robust feature of the climate system.

Keywords: Climate variability; synchronized chaos; paleoclimate.

1. Introduction

One of the most important and mysterious events in recent climate history is the climate shift in the mid-1970s [Graham, 1994]. In the northern hemisphere 500-hPa atmospheric flow the shift manifested itself as a collapse of a persistent wave-3 anomaly pattern and the emergence of a strong wave-2 pattern. The shift was accompanied by sea-surface temperature (SST) cooling in the central Pacific and warming off the coast of western North America [Miller *et al.*, 1994]. The shift brought sweeping long-range changes in the climate of northern hemisphere. Incidentally, after "the dust settled", a new long era of frequent El Niño events superimposed on a sharp global temperature increase began. While several possible triggers for the shift have been suggested and investigated [Graham, 1994; Miller *et al.*, 1994; Graham *et al.*, 1994], the actual physical mechanism that led to this shift is not known. Understanding the dynamics of such phenomena is essential for our ability to make useful prediction of climate change. A major obstacle to this understanding is the extreme complexity of the climate system, which makes it difficult to disentangle causal connections leading to the observed climate behavior. Here, we extend the analysis which has revealed an important new mechanism in climate dynamics and explained several aspects

of the observed climate variability in the late 20th century.

2. Methods and Results From Observations

First, a network consisting of four major climate indices was constructed. The network approach to complex systems is a rapidly developing methodology, which has proven to be useful in analyzing such systems behavior [Albert & Barabasi, 2002; Strogatz, 2001]. In this approach, a complex system is presented as a set of connected nodes. The collective behavior of all the nodes and links (the topology of the network) describes the dynamics of the system and offers new ways to investigate its properties. The indices represent the Pacific Decadal Oscillation (PDO), the North Atlantic Oscillation (NAO), the El Niño/Southern Oscillation (ENSO), and the North Pacific Index (NPI) [Barnston & Livezey, 1987; Hurell, 1995; Mantua *et al.*, 1997; Trenberth & Hurrell, 1994]. These indices represent regional but dominant modes of climate variability, with time scales ranging from months to decades. NAO and NPI are the leading modes of surface pressure variability in northern Atlantic and Pacific Oceans, respectively, the PDO is the leading mode of SST variability in the northern Pacific and ENSO is a major signal in the tropics. Together these four modes capture the essence of climate variability in the northern hemisphere. Each of these modes involves different mechanisms over different geographical regions. Thus, these modes are treated as nonlinear subsystems of the grand climate system exhibiting complex dynamics. Indeed, some of their dynamics have been adequately explored and explained by simplified models, which represent subsets of the complete climate system and which are governed by their own dynamics [Elsner & Tsonis, 1993; Schneider *et al.*, 2002; Marshall *et al.*, 2001; Suarez & Schopf, 1998]. For example, ENSO has been modeled by a simplified delayed oscillator in which the slower adjustment time-scales of the ocean supply the system with the memory essential to oscillation. Monthly-mean values in the interval 1900–2000 are available for all indices (http://jisao.washington.edu/datasets, for NAO, PDO and El Niño, http://www.cgd.ucar.edu/cas.jhurrell/indices.html for NPI).

These four climate indices are assumed to form a network of interacting nodes [Tsonis *et al.*, 2007]. A commonly used measure to describe variations in the network's topology is the mean distance $d(t)$ [Onnela *et al.*, 2005]

$$d(t) = \frac{2}{N(N-1)} \sum_{d_{ij}^t \in D^t} d_{ij}^t. \tag{1}$$

Here t denotes the time in the middle of a sliding window of width Δt, $N = 4$; $i, j = 1, \ldots, N$, and $d_{ij}^t = \sqrt{2(1 - |\rho_{ij}^t|)}$, where ρ_{ij}^t is the cross-correlation coefficient between nodes i and j in the interval $[t - (\Delta t - 1)/2, t + (\Delta t - 1)/2]$, and D^t is the $N \times N$ distance matrix. The sum is taken over the upper triangular part (or the distinct elements of D^t). The above formula uses the absolute value of the correlation coefficient because the choice of sign of indices is arbitrary. The distance can be thought as the average correlation between all possible pairs of nodes and is interpreted as a measure of the synchronization of the network's components. Synchronization between nonlinear (chaotic) oscillators occurs when their corresponding signals converge to a common, albeit irregular, signal. In this case, the signals are identical and their cross-correlation is maximized. Thus, a distance of zero corresponds to a complete synchronization and a distance of $\sqrt{2}$ signifies a set of uncorrelated nodes.

Figure 1(a) shows the distance as a function of time for a window length of $\Delta t = 11$ years, with tick marks corresponding to the year in the middle of the window. The correlations (and thus distance values for each year) were computed based on the annual-mean indices constructed by averaging the monthly indices over the period of November–March. The dashed line parallel to the time axis in Fig. 1(a) represents the 95% significance level associated with the null hypothesis that the observed indices are sampled from a population of a four-dimensional AR-1 process driven by a spatially (cross-index) correlated Gaussian noise; the parameters of the AR-1 model and the covariance matrix of the noise are derived from the full time series of the observed indices. This test assumes that the variations of the distance with time seen in Fig. 1(a) are due to sampling associated with a finite-length (11-yr) sliding window used to compute the local distance values. Retaining overall cross-correlations in constructing the surrogates makes this test very stringent (it is more likely that more synchronization events will be found if the surrogates were white noise, for example). It is found that five times (1910's, 1920's, 1930's, 1950's and 1970's) distance variations fall below the 95% significance level (which corresponds

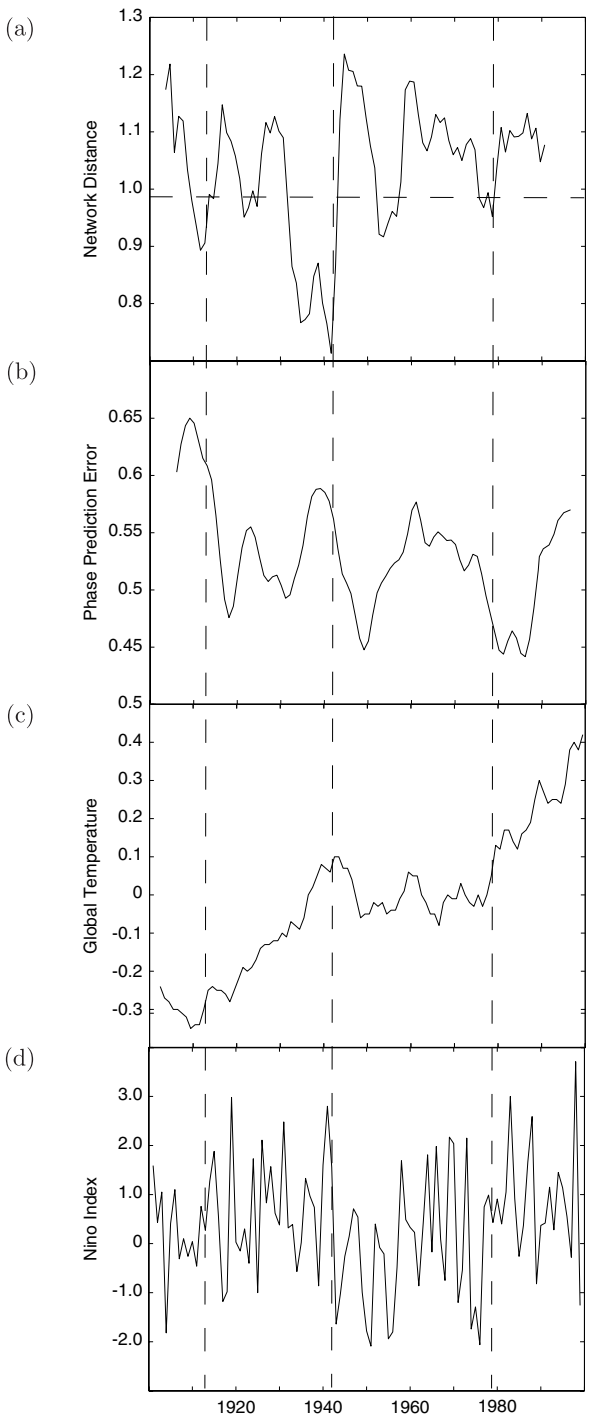

Fig. 1. (a) The distance (see definition in text) of a network consisting of four observed major climate modes as a function of time. This distance is an indication of synchronization between the modes with smaller distance implying stronger synchronization. The parallel dashed line represents the 95% significance level associated with a null hypothesis of spatially correlated red noise. (b) Coupling strength between the four modes as a function of time. (c) The global surface temperature record. (d) Global-SST ENSO index. The vertical lines indicate the time when the network goes out of synchronization for those cases where synchronization is followed by a coupling strength increase.

to an average correlation between all pairs of indices of 0.5 or greater; see Eq. (1)). It is therefore concluded that these features are not likely to be due to sampling limitations but they represent statistically significant synchronization events. Note that the window length used in Fig. 1(a) is a compromise between being long enough to estimate correlations but not too long to dilute transitions. Nevertheless, the observed synchronizations are insensitive to the window size in a wide range of $7\,\mathrm{yr} \leq \Delta t \leq 15\,\mathrm{yr}$.

An important aspect in the theory of synchronization between coupled nonlinear oscillators is coupling strength. It is vital to note that synchronization and coupling are not interchangeable; for example, it is trivial to construct a pair of coupled simple harmonic oscillators whose displacements are in quadrature (and hence perfectly uncorrelated), but whose phases are strongly coupled [Vanassche *et al.*, 2003]. As such, coupling is best measured by how strongly the phases of different modes of variability are linked. The theory of synchronized chaos predicts that in many cases when such systems synchronize, an increase in coupling between the oscillators may destroy the synchronous state and alter the systems behavior [Heagy *et al.*, 1995; Pecora *et al.*, 1997]. In view of the results above, the question thus arises as to how the synchronization events in Fig. 1(a) relate to coupling strength between the nodes. It should be noted that in this study we are interested in the complete synchronization among the nodes, rather than weaker types of synchronization, such as phase synchronization [Boccaletti *et al.*, 2002; Maraun & Kurths, 2005] or clustered synchronization [Zhou & Kurths, 2006], which are also important in climate interactions.

For our purposes here, if future changes in the phase between pairs of climate modes can be readily predicted using only information about the current phase, those modes may be considered strongly coupled [Smirnov & Bezruchko, 2003]. Here coupling is studied using symbolic dynamics. For any given time series value, we can define a symbolic phase by examining the relationship between that value and its nearest two neighbors in time. As shown in Fig. 2, if the three values are sequentially increasing, we can assign to the middle point a phase of 0, while if they are sequentially decreasing, a phase of π. Intermediate values then follow. Notice that this procedure is totally nonparametric, as it does not compare the actual values of the points aside from whether a point is larger or smaller than

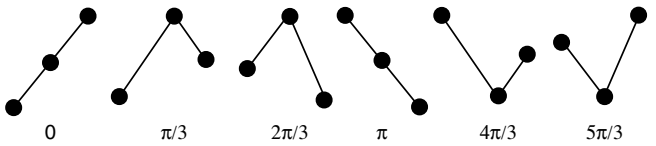

Fig. 2. The six states for the symbolic phase construction. The points in each triplet correspond to three consecutive points in a time series, and their relative vertical positions to each other indicate their respective values.

its neighbors. The advantage of this approach is that it is blind to ultra-low frequency variability, i.e. decadal scale and longer. Use of symbolic dynamics is appropriate in this case, as we are primarily interested in changes in the synchronization and coupling of climate modes over decadal time scales. The symbolic phase ϕ_n^j is constructed separately for the four climate indices, where j denotes the index and n the year. The phases for a given year n are represented by the complex phase vector $\mathbf{Z}$ with elements $Z_n^j = \exp(i\phi_n^j)$. The predictability of this phase vector from year to year provides a measure of the coupling and is determined using the least squares estimator

$$\mathbf{Z}_{n+1}^{\text{est}} = \mathbf{M}\mathbf{Z}_n \tag{2}$$

where $\mathbf{M} \equiv [\mathbf{Z}_+\mathbf{Z}^T][\mathbf{Z}\mathbf{Z}^T]^{-1}$ is the least squares predictor. Here $\mathbf{Z}$ and $\mathbf{Z}_+$ are the matrices whose columns are the vectors $\mathbf{Z}_n$ and $\mathbf{Z}_{n+1}$, respectively, constructed using all years. A measure of the coupling then is simply $\|\mathbf{Z}_{n+1}^{\text{est}} - \mathbf{Z}_{n+1}\|^2$, where strong coupling is associated with small values of this quantity, i.e. good phase prediction. Note that only three values are used to define phases rather than four or five or any other number. The reason is that the possible number of permutations of m values is $m!$. Thus, if $m > 3$ there are at least 24 possible permutations, which will not result in large sample sizes to evaluate the predictability of the phase vector.

This quantity is plotted in Fig. 1(b). Figures 1(c) and 1(d) show the global surface temperature (http://data.giss.nasa.gov/gistemp/) and El Niño index in our period. Figure 1 tells a remarkable story. First let us consider the event in 1910's. The network synchronizes at about 1910. At that time, the coupling strength begins to increase. Eventually, the network comes out of the synchronous state sometime in late 1912 early 1913 (marked by the left vertical line). The destruction of the synchronous state coincides with the beginning of a sharp global temperature increase and a tendency for more frequent and strong El Niño events. The network enters a new synchronization state in the early 1920's but this is not followed by an increase in coupling strength. In this case, no major shifts are observed in the behavior of global temperature and ENSO. Then the system enters a new synchronization state in the early 1930's. Initially this state was followed by a decrease in coupling strength and again no major shifts are observed. However, in the early 1940's, the still present synchronous state is subjected to an increase in coupling strength, which soon destroys it (at the time indicated by the middle vertical line). As the synchronous state is destroyed, a new shift in both temperature trend and ENSO variability is observed. The global temperature enters a cooling regime and El Niño events become much less frequent and weaker. The network synchronizes again in the early 1950's. This state is followed by a decrease in coupling strength and, as was the case in 1920's, no major shifts occur. Finally, the network synchronizes again in the mid 1970's. This state is followed by an increase in coupling strength and incredibly, as in the cases of 1910 and 1940, synchronization is destroyed (at the time marked by the right vertical line) and then climate shifts again. The global temperature enters a warming regime and El Niño events become frequent and strong. The fact that around 1910, 1940 and in the late 1970s climate shifted to a completely new state indicates that synchronization followed by an increase in coupling between the modes leads to the destruction of the synchronous state and the emergence of a new state.

The above mechanism was also found in three climate simulations. The first two are from the GFDL CM2.1 coupled ocean/atmosphere model [GFDL CM2.1 development team, 2006]. The first simulation is an 1860 pre-industrial conditions 500-year control run and the second is the SRESA1B, which is a business as usual scenario with CO_2 levels stabilizing at 720 ppmv at the close of the 21st century [IPCC, 2001]. The third simulation is a control run from the ECHAM5 model [Wang *et al.*, 2009]. From these model outputs the same indices were constructed (in the periods of 100–200 years, 21st century, and years 240–340, respectively) and the above procedure was repeated in order to study synchronization and coupling in the corresponding networks. In all, seven synchronization events in the model simulations occurred. Without an exception, in all cases when the major

modes of variability in the northern hemisphere are synchronized, an increase in the coupling strength destroys the synchronous state and causes climate to shift to a new state. Importantly the mechanism is found in both forced and unforced simulations indicating that the mechanism is a result of the natural variability of the climate system. Lately Swanson and Tsonis [2009] extended the analysis to the updated observations in the 21st century and discovered yet another consistent event signaling a new climate shift in the beginning of the 21st century.

The shifts described above are based on careful visual examination of the results. Once shifts have been visually identified, one can statistically test their significance. From the above results it was observed [Tsonis *et al.*, 2007; Wang *et al.*, 2009] that most often a shift in global temperature can manifest itself as a trend change but in a couple of cases it shows as a jump. Changes in ENSO variability on the other hand can come in more ways. In this case, the possible regimes are five. A regime of more frequent El Niño events, a regime of more frequent La Niña events, a regime of alternating strong El Niño and La Niña events, a regime of no activity or alternating weak El Niño and La Niña events, and a regime where the spacing between El Niño and La Niña events is irregular. In all those regimes the distribution of ENSO index is different and as such the Mann–Whitney rank sum test can be used to test for differences before and during a shift or between shifts. The same test can be used to test differences in global temperature tendency before and after a jump. In cases when a temperature tendency shift manifests itself as a trend change the t-test can be used. In all, 12 synchronization events and eight shifts occurred in observations and model simulations (not including the suspected shift in the 21st century observations). For all shifts (three in observations and five in the models), it was found that the change in ENSO variability is significant at the 90% or higher confidence level whereas the change in temperature tendency is significant at the 95% or higher confidence level [Wang *et al.*, 2009, supplementary material].

3. Results From Proxy Data

It is desirable to investigate whether this mechanism can be found in data before the 20th century. In order to do this we need to resort to proxy data. Unfortunately, data for the NPI index do not exist before the 20th century. Thus, the network of the other three modes (NAO, PDO, and ENSO) will be considered. The PDO proxy covers the period 993–1995 AD [MacDonald & Case, 2005], the NAO proxy covers the period 1049–1995 AD [Trouet *et al.*, 2009], and the ENSO proxy is [Cook *et al.*, 2009] 3.4 index in the period 1300–2005 AD. As a global temperature proxy we considered the northern hemisphere temperature reconstruction of Crowley [2000] covering the period 1000–1993 AD.

First, the overlapping period 1300–1900 AD is considered (here the period 1900–2007 AD where instrumental measurement exist and have been analyzed previously is not considered). Then the network is constructed and as previously the synchronization measure and coupling are computed. The results are shown in Fig. 3. In the top panel, the synchronization measure is shown. This measure is a simplified version of Eq. (1) (it is the root mean square of the cross-correlation coefficient between all unique pairs of the three indices; in this way, unlike in Fig. 1(a), higher values indicate synchronization). The window over which the correlations are estimated is 21 years (rather than 11 used in the previous studies). A wider window compensates for the increased uncertainty in proxy records. According to a similar surrogate data analysis, a value above 0.31 indicates a statistically significant synchronization event. The middle panel shows the coupling measure as modified in [Swanson & Tsonis, 2009]. As before when this measures decreases, coupling strength increases. We find that the mechanism of synchronization + increase (decrease) in coupling → climate shift (no climate shift) is again present, but it is not as robust as in the previous results. It is observed in 17 out of the total 23 synchronization events in that period (a 75% success rate). In three synchronization events the coupling was increasing but no shift occurred and in three other events the coupling was decreasing but a shift did occur. This "departure" from the robustness of the mechanism observed in the modern data and in model simulations may be due to the fact that the proxy data are not as reliable as actual measurements and/or because this network has three of the four modes used in the previous studies. Sensitivity analysis using a network constructed from the observations in the 20th century but without the NPI lowers the success rate in that period from five out of five to four out of five. Thus, not having NPI may be part of the problem. However, the small sample size of synchronization

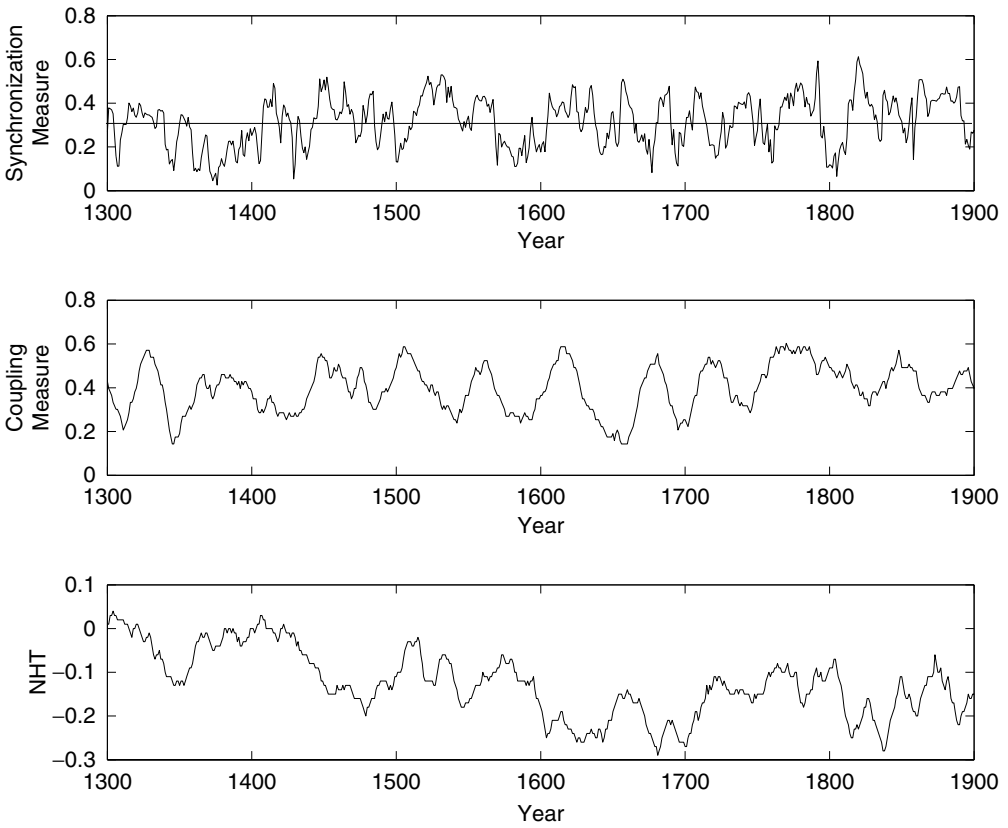

Fig. 3. The top panel shows the synchronization measure. This measure is a simplified version of Eq. (1) [it is the root mean square of the cross-correlation coefficient between all unique pairs of the three indices; in this way, unlike in Fig. 1(a), higher values indicate synchronization]. The window over which the correlations are estimated is 21 years. According to surrogate data analysis a value above 0.31 (horizontal solid line) indicates a statistically significant synchronization event. Twenty three synchronization events are observed in the period 1300–1900. The middle panel shows the coupling measure as modified in [Swanson & Tsonis, 2009]. Here again, when this measures decreases, coupling strength increases. The bottom panel is the NH temperature proxy used in this study.

events inhibits us from making concrete conclusions on this issue. It is nevertheless encouraging that the mechanism is observed in 17 out of 23 synchronization events. In order to further support the statistical significance of the existence of the mechanism in the proxy data we adopted a different approach. More specifically we examined the coherence between synchronization measure, coupling measure, and NH temperature.

Coherence measures the linear dependence of the oscillatory components in the two detrended signals. While it does not indicate cause and effect, significant coherence suggests that changes in one signal relate to changes in the other signal. When the squared coherency is transformed by the inverse hyperbolic tangent, the resulting values have a normal distribution centered on zero and with a variance proportional to the sum of squares of the smoothing weights [Kuo *et al.*, 1990]. This allows us to make a correspondence between the values of squared coherency and confidence levels. For example, for a given frequency, squared coherency values of 0.2, 0.25 and 0.31 define the approximate 90%, 95% and 99% confidence levels, respectively, for incoherent series.

Estimation of the magnitude square coherence is based on Matlab's program `mscohere`. The programs computes the magnitude squared coherence estimate C_{xy} of the input signals x and y using Welch's averaged, modified periodogram method [Welch, 1967]. The magnitude squared coherence estimate is a function of frequency with values between 0 and 1 that indicates how well x corresponds to y at each frequency. The magnitude squared coherence is a function of the power spectral densities ($P_{xx}(f)$ and $P_{yy}(f)$) of x and y and the cross power spectral density ($P_{xy}(f)$) of x and y,

$$C_{xy}(f) = \frac{|P_{xy}(f)|^2}{P_{xx}(f)P_{yy}(f)}, \tag{3}$$

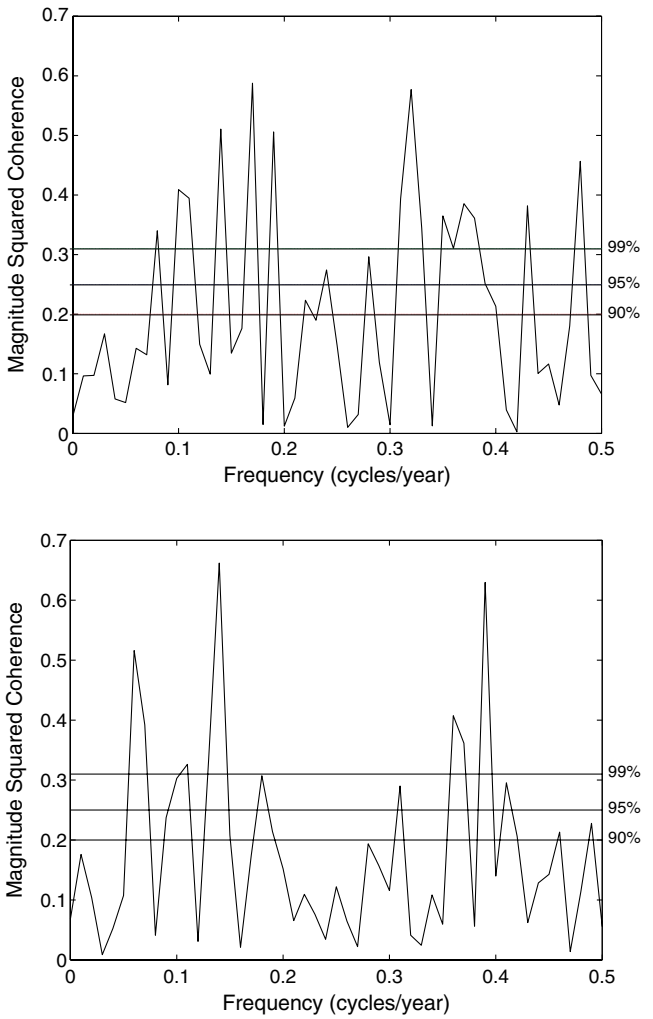

Fig. 4. Magnitude square coherence between coupling and NH temperature (top) and between distance and NH temperature (bottom). Both figures indicate significant coherence at several frequencies. See text for details.

where x and y must be the same length. For real x and y, the program returns a one-sided coherence estimate and for complex x or y, it returns a two-sided estimate.

Figure 4 shows the magnitude square coherence between coupling and temperature (top) and between distance and NH temperature (bottom). Both figures indicate significant coherence at several frequencies. More specifically, the top panel shows significant coherence between coupling and NHT over a range of frequencies centered at about 0.15 cycles/year (corresponding to a time scale of 7–8 years) and a range of frequencies centered at about 0.33 cycles/year (corresponding to a time scale of 3 years). The bottom panel shows significant coherence between distance and NHT over a range of frequencies centered at about 0.1 cycles/year (corresponding to a time scale of 10 years) and a range of frequencies centered at about 0.4 cycles/year (corresponding to a time scale of 2.5 years). Phase estimates are not clear because the duration of both synchronization and coupling strength increase varies from case to case, but it appears that both distance and coupling lead NHT. These results are consistent with the proposed mechanism for major climate shifts. In the low frequency domain the time scale in the coherence between distance and NHT is longer than that between coupling and NHT. This is a direct result of the fact that according to the mechanism for a shift to take place the modes must first synchronize and then coupling must increase. In this case, coupling increase acts for a shorter time period compared to the length of synchronization. The opposite is observed over the higher frequency ranges. As is shown in Fig. 3 the synchronization measure exhibits more high frequency variability than the coupling measure. Thus, in some cases synchronization may begin while coupling is increasing and the event may not last sufficiently long to change the climate state. Nevertheless, this is not inconsistent with synchronization + coupling increase (decrease) $\rightarrow$ climate shift (no climate shift).

4. Conclusions

According to the Tsonis–Swanson–Kravtsov (TSK) mechanism for major climate shifts [Tsonis *et al.*, 2007] major climate modes tend to synchronize at some coupling strength. When this synchronous state is followed by an increase in the coupling strength, the networks' synchronous state is destroyed and after that climate emerges in a new state. The whole event marks a significant shift in climate. Here, we have performed an analysis of proxy climate data in order to further investigate the validity of the TSK mechanism beyond the time of the actual instrumental records. Again, we find strong evidence of the mechanism as well as significant coherence between both synchronization and coupling and global temperature. These results provide further support that the above mechanism for climate shifts is a robust feature of the climate system.

Acknowledgment

This work is supported by NSF grant AGS — 0902564.

References

Albert, R. & Barbasi, A.-L. [2002] "Statistical mechanics of complex networks," *Rev. Mod. Phys.* **74**, 47–101.

Barnston, A. G. & Livezey, R. E. [1987] "Classification, seasonality, and persistence of low-frequency atmospheric circulation patterns," *Mon. Wea. Rev.* **115**, 1083–1126.

Bocaletti, S., Kurths, J., Osipov, G., Valladres, D. J., Zhou, C. S. & Livezey, R. E. [2002] "The synchronization of chaotic systems," *Phys. Rep.* **366**, 1–101.

Cook, E. R. *et al.* [2009] "Tree Ring 700 Year ENSO index reconstructions," *IGBP PAGES/World Data Center for Paleoclimatology Data Contribution Series # 2009–105.* NOAA/NCDC Paleoclimatology Program, Boulder CO, USA.

Crowley, T. J. [2000] "Causes of climate change over the past 1000 years," *Science* **289**, 270–277.

Elsner, J. B. & Tsonis, A. A. [1993] "Nonlinear dynamics established in the ENSO," *Geophys. Res. Lett.* **20**, 213–216.

GFDL CM2.1 development team [2006] "GFDLs CM2 global coupled climate models, Parts 1–4," *J. Clim.* **19**, 643–740.

Graham, N. E. [1994] "Decadal scale variability in the tropical and North Pacific during the 1970s and 1980s: Observations and model results," *Clim. Dyn.* **10**, 135–162.

Graham, N. E., Barnett, T. P., Wilde, R., Pnoater, M. & Schubert, S. [1994] "On the roles of tropical and midlatitude SSTs in forcing interannual to interdecadal variability in the winter Northern Hemisphere circulation," *J. Clim.* **7**, 1500–1515.

Heagy, J. F., Pecora, L. M. & Carroll, T. L. [1995] "Short wavelength bifurcations and size instabilities in coupled oscillator systems," *Phys. Rev. Lett.* **74**, 4184–4188.

Hurrell, J. W. [1995] "Decadal trends in the North Atlantic oscillation regional temperature and precipitation," *Science* **269**, 676–679.

IPCC [2001] *Climate Change 2001 — The Scientific Basis*, eds. Houghton, J. H. *et al.* (Cambridge University Press).

Kuo, C., Lindeberg, C. & Thomson, D. J. [1990] "Coherence established between atmospheric carbon dioxide and global temperature," *Nature* **343**, 709–714.

MacDonald, G. M. & Case, R. A. [2005] "Variations in the Pacific Decadal oscillation over the past millennium," *Geophys. Res. Lett.* **32**, L08703.

Mantua, N. J., Hare, S. R., Zhang, Y., Wallace, J. M. & Francis, R. C. [1997] "A Pacific interdecadal climate oscillation with impacts on salmon production," *Bull. Am. Met. Soc.* **78**, 1069–1079.

Maraun, D. & Kurths, J. [2005] "Epochs of phase coherence between El Niño/Southern oscillation and Indian monsoon," *Geophys. Res. Lett.* **32**, L15709.

Marshall, J. *et al.* [2001] "North Atlantic climate variability: Phenomena, impacts and mechanisms," *Int. J. Climatol.* **21**, 1863–1898.

Miller, A. J., Cayan, D. R., Barnett, T. P., Craham, N. E. & Oberhuber, J. M. [1994] "The 1976–77 climate shift of the Pacific Ocean," *Oceanography* **7**, 21–26.

Onnela, J.-P., Saramaki, J., Kertesz, J. & Kaski, K. [2005] "Intensity and coherence of motifs in weighted complex networks," *Phys. Rev. E* **71**, 065103.

Pecora, L. M., Carroll, T. L., Johnson, G. A. & Mar, D. J. [1997] "Fundamentals of synchronization in chaotic systems, concepts, and applications," *Chaos* **7**, 520–543.

Schneider, N., Miller, A. J. & Pierce, D. W. [2002] "Anatomy of North Pacific decadal variability," *J. Clim.* **15**, 586–605.

Smirnov, D. A. & Bezruchko, B. O. [2003] "Estimation of interaction strength and direction from short and noisy time series," *Phys. Rev. E* **68**, 046209.

Strogatz, S. H. [2001] "Exploring complex networks," *Nature* **410**, 268–276.

Suarez, M. J. & Schopf, P. S. [1998] "A delayed action oscillator for ENSO," *J. Atmos. Sci.* **45**, 549–566.

Swanson, K. L. & Tsonis, A. A. [2009] "Has the climate recently shifted?" *Geopys. Res. Lett.* **36**, L06711.

Trenberth, K. E. & Hurrell, J. W. [1994] "Decadal atmospheric-ocean variations in the Pacific," *Clim. Dyn.* **9**, 303–319.

Trouet, V., Esper, J., Graham, N. E., Baker, A., Scourse, J. D. & Frank, D. C. [2009] "Persistent positive North Atlantic oscillation mode dominated the medieval climate anomaly," *Science* **324**, 78–80.

Tsonis, A. A., Swanson, K. L. & Kravtsov, S. [2007] "A new dynamical mechanism for major climate shifts," *Geophys. Res. Lett.* **34**, L13705.

Vannassche, P., Gielen, G. G. E. & Sansen, W. [2003] "Behavioral modeling of (coupled) harmonic oscillators," *IEEE Trans. Comp. Des. Int. Circ.* **22**, 1018–1027.

Wang, G., Swanson, K. L. & Tsonis, A. A. [2009] "The pacemaker of major climate shifts," *Geophys. Res. Lett.* **36**, L07708.

Welch, P. D. [1967] "The use of fast Fourier transform for the estimation of power spectra: A method based on time averaging over short, modified periodograms," *IEEE Trans. Audio Electroacous.* **AU-15**, 70–73.

Zhou, C. S. & Kurths, J. [2006] "Dynamical weights and enhanced synchronization in adaptive complex networks," *Phys. Rev. Lett.* **96**, 164102.